Title

Investigating calcite growth rates using a quartz crystal microbalance with dissipation (QCM-D)

Permalink

Authors

Cao, Bo
Stack, Andrew G
Steefel, Carl I
et al.

Publication Date

2018-02-01

DOI

10.1016/j.gca.2017.10.020

Investigating calcite growth rates using a quartz crystal microbalance with dissipation (QCM-D)

Author links open overlay panel Bo Cao[a] Andrew G. Stack[b] Carl I. Steefel[c] Donald J. DePaolo[c] Laura N. Lammers[d] Yandi Hu[a]
Show more

https://doi.org/10.1016/j.gca.2017.10.020 Get rights and content

Abstract

Calcite precipitation plays a significant role in processes such as geological carbon sequestration and toxic metal sequestration and, yet, the rates and mechanisms of calcite growth under close to equilibrium conditions are far from well understood. In this study, a quartz crystal microbalance with dissipation (QCM-D) was used for the first time to measure macroscopic calcite growth rates. Calcite seed crystals were first nucleated and grown on sensors, then growth rates of calcite seed crystals were measured in real-time under close to equilibrium conditions (saturation index, SI = log ($\{Ca^{2+}\}/\{CO_3^{2-}\}/K_{sp}$) = 0.01–0.7, where {i} represent ion activities and $K_{sp} = 10^{-8.48}$ is the calcite thermodynamic solubility constant). At the end of the experiments, total masses of calcite crystals on sensors measured by QCM-D and inductively coupled plasma mass spectrometry (ICP-MS) were consistent, validating the QCM-D measurements. Calcite growth rates measured by QCM-D were compared with reported macroscopic growth rates measured with auto-titration, ICP-MS, and microbalance. Calcite growth rates measured by QCM-D were also compared with microscopic growth rates measured by atomic force microscopy (AFM) and with rates predicted by two process-based crystal growth models. The discrepancies in growth rates among AFM measurements and model predictions appear to mainly arise from differences in step densities, and the step velocities were consistent among the AFM measurements as well as with both model predictions. Using the predicted steady-state step velocity and the measured step densities, both models predict well the growth rates measured using QCM-D and AFM. This study provides valuable insights into the effects of reactive site densities on calcite growth rate, which may help design future growth models to predict transient-state step densities.

- **Previous** article in issue
- **Next** article in issue

Keywords

Crystal growth rate

Calcite
Quartz crystal microbalance with dissipation
Step density
Step velocity

1. Introduction

Calcite, as a major mineral in sedimentary rocks, can precipitate in many natural and anthropogenic systems (Tucker and Wright, 1990, Morse and Arvidson, 2002, Morse et al., 2007). Quantitatively understanding the extent, location and rate of calcite precipitation provides important information on paleo-environments as well as on the geochemical processes taking place during geological carbon sequestration and toxic metal sequestration (Marshall and McCulloch, 2002, Fantle and DePaolo, 2005, Lagneau et al., 2005, Eisenhauer et al., 2009, Bracco et al., 2012, Stack, 2014). The kinetics of calcite growth as a function of solution chemistry has been studied extensively for decades by both macroscale and microscale experimental techniques. Macroscopic calcite growth rates have been determined by either monitoring solution composition changes or measuring the mass change of calcite seed crystals (Nancollas and Reddy, 1971, Reddy and Gaillard, 1981, Christoffersen and Christoffersen, 1990, Zhong and Mucci, 1993, Zuddas and Mucci, 1994, Zuddas and Mucci, 1998, Nehrke et al., 2007, Lopez et al., 2009, Gebrehiwet et al., 2012). However, some of these methods may not be able to provide real-time measurements of slow growth rates under close to equilibrium conditions. For example, Nehrke et al. (2007) used a microbalance with a resolution of 0.1 µg to measure the growth rates of a calcite seed crystal in solution at a saturation index ($SI = \log(\{Ca^{2+}\}/\{CO_3^{2-}\}/K_{sp})$, where {i} represent ion activities and $K_{sp} = 10^{-8.48}$ is the calcite thermodynamic solubility constant) of 0.70. After 266 hrs, the total mass increase of the calcite seed crystal was only 33 µg. In recent decades, calcite growth has been studied under different solution conditions using *in situ* atomic force microscopy (AFM) (Gratz et al., 1993, Teng et al., 2000, Larsen et al., 2010a, Larsen et al., 2010b, Stack and Grantham, 2010, Ruiz-Agudo et al., 2011a, Bracco et al., 2012, Bracco et al., 2013). Based on the observed steady-state step densities and step velocities, macroscopic growth rates can theoretically be inferred from these sub-microscale images. However, the growth rates calculated based on these AFM observations were limited to growth that occurred on single spirals and did not include other growth mechanisms, such as single-sourced multi-spiral growth and 2-D nucleation (Teng et al., 2000). Moreover, calcite growth and dissolution may occur simultaneously at different locations on the crystal surface (Stack and Grantham, 2010). Therefore, localized microscopic calcite growth rates measured by AFM may not necessarily represent macroscopic growth rates, which are required to predict large-scale calcite growth in geologic settings using reactive transport modeling (Steefel et al., 2005). Little has been reported on the macroscopic growth rates of calcite under close to equilibrium conditions (SI < 0.10), despite the fact that this is a common condition in natural geologic systems (Plummer, 1975, Zhong and Mucci, 1993). Zuddas and Mucci (1994)reported macroscopic calcite growth rates under atmospheric pressure condition but at relatively high solution supersaturations (SI > 0.15). Data on macroscopic calcite growth rates under close to equilibrium conditions at atmospheric pressure conditions are still extremely limited.

The quartz crystal microbalance with dissipation (QCM-D) technique can detect variations in mass as low as 0.5 ng/cm^2 on a quartz sensor, by monitoring changes in resonant frequencyand dissipation of an oscillating quartz sensor. The resonant frequency shift (Δf) is related to the mass change on the sensor (Richter and Brisson, 2004, Dixon, 2008), and the dissipation shift (ΔD) is related to the rigidity of the surface layer on the sensor (Richter and Brisson, 2004, Dixon, 2008). QCM-D has been widely utilized to investigate interactions at solid-liquid interfaces, including the adsorption of molecules (Maroni et al., 2015, Zhu et al., 2016) and ions (Dai and Hu, 2014, Dai et al., 2016a, Dai et al., 2016b) as well as the deposition of nanoparticles and biomolecules onto organic/inorganic coatings (Richter and Brisson, 2004, Höök et al., 2008, Knoll et al., 2008, Chen et al., 2016). Here, QCM-D was used for the first time to quantify macroscopic calcite crystal growth rates under close-to-equilibrium conditions.

2. Materials and methods

2.1. Setup of calcite growth experiments

Calcite growth on QCM-D sensors was conducted with a Q-Sense E4 system (Biolin Scientific) at 25.0 ± 0.1 °C using the experimental setup shown in Fig. 1. The prepared $CaCl_2$and $NaHCO_3$ solutions were placed in a water bath to keep the temperature at 25.0 ± 0.1 °C. Each solution was pumped by a peristaltic pump (IPC-N 4, Ismatec) at a flow rate of 0.125 mL/min. The $CaCl_2$ and $NaHCO_3$ solutions were mixed in a small mixing cell (volume: ∼70 µl) with magnetic stirring immediately before injection into the QCM-D chamber (temperature maintained at 25.0 ± 0.1 °C, volume: ∼40 µl).

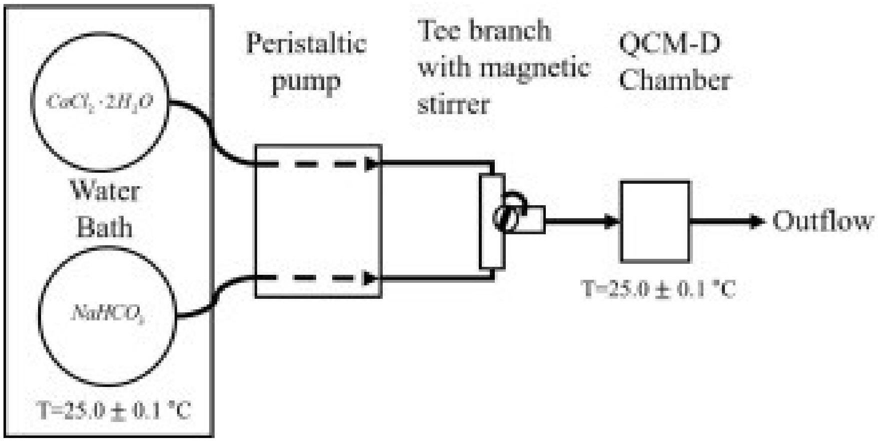

1. Download high-res image (79KB)
2. Download full-size image

Fig. 1. Schematic plot of the flow through set up for QCM-D experiments.

2.2. Solution preparation

ACS reagent grade chemicals ($CaCl_2 \cdot 2H_2O$, $NaHCO_3$) were used to prepare stock solutions of $CaCl_2$ (0.00239 M) and $NaHCO_3$ (0.155 M). Ultrapure water (18.2 MΩ·cm) was sparged with air for 24 h to ensure complete equilibration with atmospheric CO_2. Immediately before each experiment, $CaCl_2$ and $NaHCO_3$ stock solutions were weighed with a Mettler Toledo balance (0.1 mg precision) and diluted with the sparged ultrapure water to prepare separate $CaCl_2$ and $NaHCO_3$ solutions with the desired concentrations. Using PHREEQC (version 3.3.3.10424) and the thermodynamic data from the Lawrence Livermore National Library database (llnl.dat), the mixed solution compositions, pH, ion activities, and saturation indices with respect to calcite were calculated, as given in Table 1. For all experiments, the pH values (8.18–8.22) and activity ratios (0.97–1.07) of $\{Ca^{2+}\}/\{CO_3^{2-}\}$in the mixed solutions were similar. Two K_{sp} values for calcite at 25 °C, $10^{-8.54}$ (Teng et al., 1998) and $10^{-8.48}$(Plummer and Busenberg, 1982), have been used in previous studies (Plummer and Busenberg, 1982, Teng et al., 1998, Teng et al., 1999, Teng et al., 2000, Larsen et al., 2010a, Larsen et al., 2010b, Teng et al., 2011, Gebrehiwet et al., 2012, Bracco et al., 2013). In this study, QCM-D experiments were conducted using a solution with 8.46×10^{-5} M $Ca^{2+}$and 8.18×10^{-5} M CO_3^{2-} (Sample #1, Table 1). This solution is supersaturated with respect to calcite if a $K_{sp} = 10^{-8.54}$ is used, and undersaturated if a $K_{sp} = 10^{-8.48}$ is used. The QCM-D measurements reported here (Fig. A1) indicated that calcite dissolution rather than growth took place in this solution. Thus $K_{sp} = 10^{-8.48}$ was used in this study to calculate calcite supersaturations (Table 1, −0.01 to 0.70).

Table 1. Solution compositions for calcite growth experiments and the calculated growth rates. Concentration of ions ($[Ca^{2+}]$, $[CO_3^{2-}]$), activities of ions ($\{Ca^{2+}\}$, $\{CO_3^{2-}\}$), calcium/carbonate activity ratios ($\{Ca^{2+}\}/\{CO_3^{2-}\}$), saturation indices (SI) with respect to calcite, ionic strength values (IS), pH, and calculated calcite growth rates are listed.

Sample No.	$[Ca^{2+}]$ (10^{-5} M)	$[CO_3^{2-}]$ (10^{-5} M)	$\{Ca^{2+}\}$ (10^{-5})	$\{CO_3^{2-}\}$ (10^{-5})	$\{Ca^{2+}\}/\{CO_3^{2-}\}$	SI[a]	IS (mM)	pH	Calcite growth rate (10^{-2}µmol/m²/s)
# 1	8.46	8.18	5.83	5.55	1.05	−0.01	8.82	8.22	−3.1 ± 0.2
# 2	8.69	8.42	5.96	5.69	1.05	0.01	9.05	8.22	1.4 ± 0.1
# 3	8.81	8.54	6.03	5.76	1.05	0.02	9.18	8.22	3.2 ± 0.7
# 4	8.94	8.68	6.11	5.83	1.05	0.03	9.31	8.22	4.7 ± 0.6
# 5	9.06	8.81	6.18	5.91	1.05	0.04	9.44	8.22	6.4 ± 0.3
# 6	9.17	8.94	6.24	5.98	1.05	0.05	9.57	8.22	7.6 ± 0.8
# 7	9.58	9.54	6.45	6.32	1.05	0.10	10.16	8.22	13 ± 0.1
# 8	12.6	12.6	8.09	7.96	1.02	0.30	13.24	8.21	30 ± 6.4
# 9	17.1	16.4	10.5	9.93	1.07	0.50	17.12	8.20	138 ± 15
# 10	22.3	23.7	12.7	13.1	0.97	0.70	24.18	8.18	226 ± 22

a

SI = log ($\{Ca^{2+}\}/\{CO_3^{2-}\}K_{sp}$), where {i} represent ion activities and $K_{sp} = 10^{-8.48}$ is the calcite thermodynamic solubility constant.

2.3. Real-time calcite growth experiments in QCM-D chamber

QCM-D measurements were conducted in two steps (Fig. 2): first, calcite seed crystals were generated on sensors coated with OH-terminated self-assembled monolayers (SAMs) (Aizenberg et al., 1999a, Aizenberg et al., 1999b, Wang et al., 2010) at a relatively high SI = 0.70 (Step I, details in Appendix A), and second, the growth rates of calcite seed crystals were quantified under close to equilibrium conditions (Step II, SI = 0.01–0.50, Table 1). Immediately after switching feed solutions, the flow rate was increased to 1.20 mL/min for five mins to allow the new feed solutions (SI < 0.70) to fully replace the initial solution (SI = 0.70) in the system. Thereafter, the pump was adjusted back to a flow rate of 0.125 mL/min.

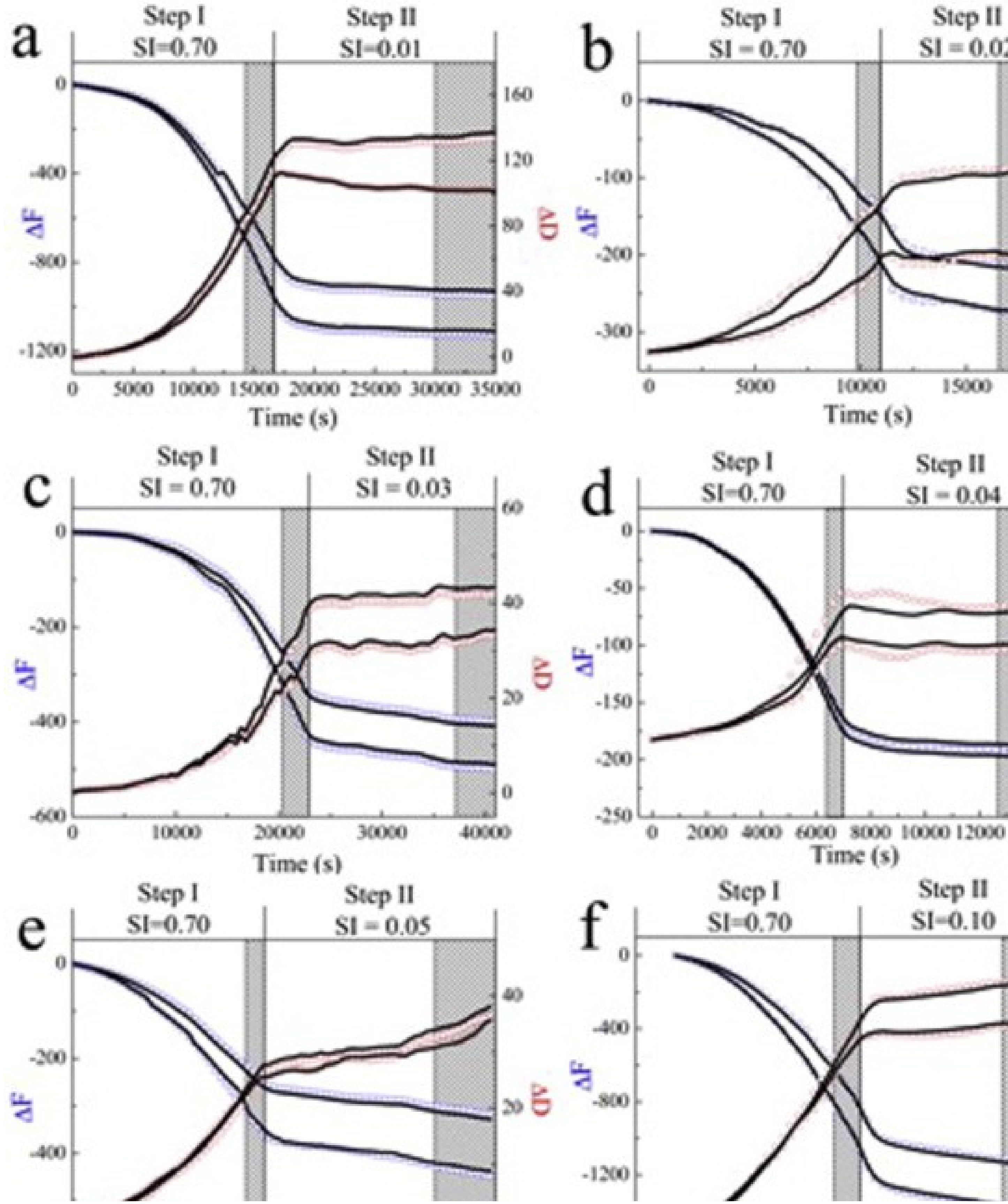

a
Step I
SI=0.70
Step II
SI=0.01
ΔF
ΔD
Time (s)
b
Step I
SI = 0.70
Step II
ΔF
Time (s)
c
Step I
SI = 0.70
Step II
SI = 0.03
ΔF
ΔD
Time (s)
d
Step I
SI=0.70
Step II
SI = 0.04
ΔF
Time (s)
e
Step I
SI=0.70
Step II
SI = 0.05
ΔF
ΔD
f
Step I
SI=0.70
Step II
SI=0.10
ΔF

1. Download high-res image (403KB)
2. Download full-size image

Fig. 2. QCM-D measurements of calcite seed crystal generation (Step I, SI = 0.70) and growth in solutions with lower SI values (Step II, SI = 0.01, 0.02, 0.03, 0.04, 0.05, 0.10, 0.30, and 0.50, Figures a-h). The blue markers indicate frequency changes shown on the left Y axis. The red markers indicate dissipation changes shown on the right Y axis. Data in shaded areas were fitted to calculate calcite growth rates, and the solid black lines were model fittings. (For interpretation of the references to colour in this figure legend, the reader is referred to the web version of this article.)

2.4. QCM-D data analysis

The real-time changes in resonant frequency (Δf) and dissipation (ΔD) of the sensors (Fig. 3) caused by calcite nucleation and growth were fitted to a Kelvin-Voigt viscoelastic model (Voinova et al., 1999) (fitted curves are shown as black lines in Fig. 3) using QTools software (Version 3.0, Biolin Scientific AB). By obtaining the best fits of the QCM-D measured frequency (Δf) and dissipation (ΔD) changes at different overtones (e.g., 15 MHz, 25 MHz, 35 MHz and 45 MHz), film viscosity, mass changes on sensors were calculated. More details of model fitting can be found in Appendix A.

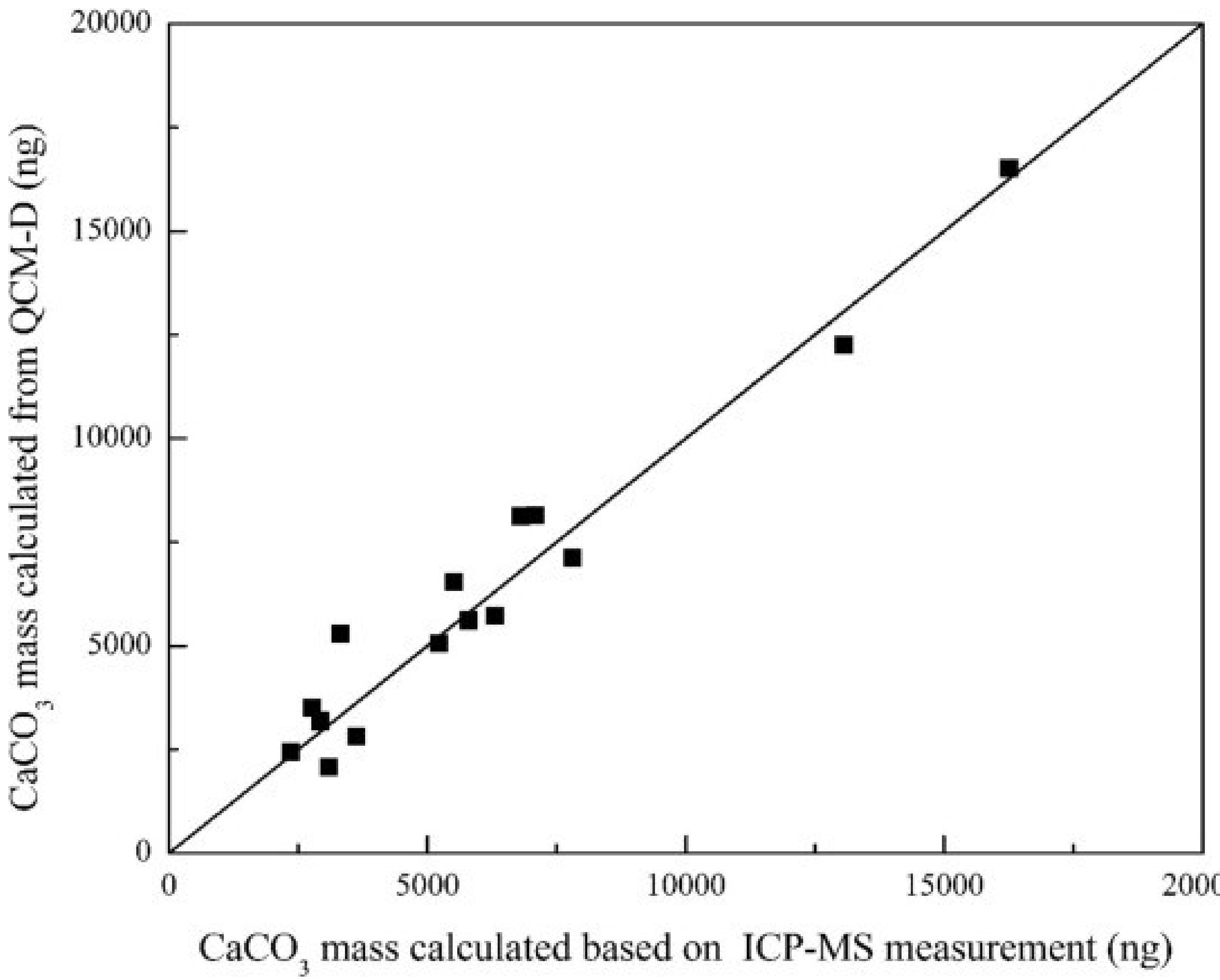

1. Download high-res image (103KB)
2. Download full-size image

Fig. 3. Calcite masses on sensors calculated from QCM-D and ICP-MS measurements.

2.5. Ex-situ characterization of calcite coverage on sensor using optical microscopy

At the end of each QCM-D experiment, the sensor was removed from the QCM-D chamber, rinsed with ethanol to remove the residual solution, and dried with N_2 gas. To quantify the surface coverage of calcite crystals on the sensor, the sensor surface was imaged by optical microscopy (Optem, Qioptiq). Using a magnification of 500, a total of 50 pictures were taken to cover the entire sensor surface. A typical image collected by the optical microscopy at 500× magnification is shown in Fig. A3. Using Image J software, the original optical image was processed to a black-and-white version (Fig.

A3) and surface coverage of the sensor by dark spots corresponding to calcite crystals was calculated. By analyzing all 50 images, the coverage of calcite crystals on the entire sensor surface was calculated, as shown in Table A1.

The sensor was only partially covered with calcite crystals (Fig. A3), with a large percentage of the sensor covered by SAM coatings. Therefore, it is possible that the mass changes recorded by the sensor during seed crystal growth (Step II) may be partially generated by ion adsorption and/or the nucleation of additional calcite on the SAMs. To investigate such effects, control experiments were conducted using the same flow system (Fig. 1), but by directly flowing a solution with SI = 0.30 or 0.50 over a SAM-coated sensor without calcite seed crystals. Minor changes in frequency and dissipation were observed over 4 hours for both conditions (Fig. A4), and the calculated mass change attributed to ion adsorption and calcite nucleation on SAM coatings was less than 5% of the mass increase observed during the growth of seed crystals under the same solution conditions (Step II, Fig. 2). Thus, we concluded that the measured mass increases during Step II (Fig. 2) were mainly caused by the growth of preexisting calcite seed crystals.

2.6. Ex situ characterization of calcite amount on sensors using ICP-MS

After quantifying the surface coverage of seed crystals on the sensor, the sensor was soaked in a 5.00 mL 1.0% HCl solution in a test tube. The test tube was then placed on a shaker (Innova 2000, Expotech) at a speed of 100 rpm for 24 hours to dissolve all calcite seed crystals. The dissolved Ca concentration was measured by inductively coupled plasma mass spectrometry (ICP-MS, PerkinElmer) with an analytical error of ∼10% and a detection limit of ∼10 µg/L. The total mass of calcite crystals on the sensor was calculated from the Ca concentration.

2.7. Calcite step density measurement using vertical scanning interferometer (VSI)

Step densities on the calcite surface, which can affect its growth rate significantly, have been measured using AFM in previous studies with calcite crystals (Teng et al., 1998, Teng et al., 2000, Stack and Grantham, 2010, Bracco et al., 2012, Bracco et al., 2013). In this study, the seed crystals generated on the Au sensors were very small (∼1–5 µm), making it difficult to perform AFM measurements. Vertical scanning interferometry (VSI, NewView™ 7300, Zygo) has been utilized to quantify the changes in surface roughness during glass dissolution (Icenhower and Steefel, 2015), and was used here to measure the step densities after growth experiments (Step II). A similar two-step procedure was followed: First, a gold wafer coated with –OH terminated

SAMs was immersed in a mixed $CaCl_2$ and $NaHCO_3$ solution (SI = 1.50) for 12 hrs for seed crystal generation. The mixed solution with a higher SI (1.50 instead of 0.70) was able to generate bigger seed crystals (∼20–30 μm, Fig. A5) for high-quality VSI measurements. Second, the gold wafer was immersed with solutions having SI = 0.02, 0.06, 0.10, 0.20, 0.30, 0.40, 0.50, or 1.00 for 1 h (Step II). Finally, the step densities of calcite crystals after the growth in lower SI solutions (Step II) were measured by VSI (Fig. A5). The detailed experimental procedure for VSI measurements can be found in Appendix A. The measured VSI step densities shown in Fig. A6 were fitted to an empirical expression:

(1) $\rho_{step} = y_0 + A\exp(-SI/\tau)$

where y_0, A and τ are fitting parameters, and each data point was weighted by its standard deviation. The fit obtained was excellent, as shown in Fig. A6, but it should be noted that the solution used to generate the larger seed crystals required for VSI measurement had a higher supersaturation (SI = 1.50) than the solution used to generate seed crystals (SI = 0.70) for QCM-D experiments. Therefore, the step densities measured via VSI may not exactly correspond to the step densities of calcite seed crystals on QCM-D sensors.

3. Results

3.1. Validation of QCM-D measurements: comparison of total calcite mass measured by QCM-D and ICP

The full data sets of real-time QCM-D results under our experimental conditions (with seed crystal generation under SI = 0.70 and later crystal growth under SI = 0.01, 0.02, 0.03, 0.04, 0.05, 0.10, 0.30, 0.50) are shown in Fig. 2. During both the seed crystal generation (SI = 0.70, Step I) and the later crystal growth (SI = 0.01, 0.02, 0.03, 0.04, 0.05, 0.10, 0.30, 0.50, Step II), decreases in frequency (blue markers in Fig. 2) and increases in dissipation (red markers in Fig. 2) are observed, indicating mass increases on sensors caused by calcite nucleation and growth.

The real-time evolution of total calcite mass per unit surface area on the sensor was calculated by the *Kelvin-Voigt* viscoelastic model (Voinova et al., 1999) (Table A1). By multiplying the surface area of the sensor in contact with the solution (7.70×10^{-5} m^2), the total mass of calcite crystals on the sensor surface at the end of each experiment was calculated, as plotted on the Y-axis of Fig. 3. The total mass of calcite on the sensor at the end of each experiment calculated from the ICP-MS measurements is plotted on the X-axis of Fig. 3. All the data points fall along a 1:1 line (Fig. 3), indicating that the total calcite mass on the sensor measured by QCM-D was consistent with the mass calculated from ICP-MS analysis. This good agreement demonstrates the validity of using the *Kelvin-Voigt*viscoelastic model to quantify crystal growth on sensors. It should be noted that, whereas it was possible to measure the total masses of calcite crystals after growth experiments using ICP-MS, this technique is not suitable to determine the real-time change of dissolved Ca concentrations and the corresponding real-time calcite growth rates under close to equilibrium conditions (SI < 0.10).

3.2. Calcite growth rates determined by QCM-D

The real-time QCM-D data of calcite seed crystal generation (Step I) and later growth (Step II) are shown in Fig. 2. For Step I (SI = 0.70), the initial slow changes in frequency and dissipation (Fig. 2) indicated the slow nucleation of calcite seed crystals on the sensor. With the generation of a larger number of calcite seed crystals, a more rapid mass increase on the sensor was observed, indicating that calcite growth became the dominant mechanism of mass increase. For Step II, when the feed solutions were switched from SI = 0.70 to lower SI (Fig. 2), the parabolic curves of frequency and dissipation changes indicated that the calcite growth rates started to decrease after switching to the growth solution with lower SI. For both Steps I and II (Fig. 2), after the initial parabolic curves of frequency and dissipation changes with time, linear curves (indicated by the shaded areas in Fig. 2) were established. The calcite mass increase (Δm, μg/m^2) over time (t, seconds) under both SI = 0.70 and SI = 0.01, 0.02, 0.03, 0.04, 0.05, 0.10, 0.30, 0.50 were calculated based on the fittings of data in shaded areas, as shown in Table A1.

In the *Kelvin-Voigt* viscoelastic model, the calculated mass increase (Δm, μg/m^2) over time (t) was normalized to the entire sensor surface area, but calcite crystals only partially covered the sensors (Fig. A2). In addition, the seed crystals grown on sensors were rhombohedral, and therefore had five $10\bar{1}4$ surfaces exposed to the solution. Two simplifications were made here to calculate the calcite surface area for growth rate normalization: (1) all five $10\bar{1}4$ surfaces had the same surface area; (2) change in crystal surface area during the slow growth period (shaded areas of Step II, Fig. 2) was insignificant, as the mass increase (Δm, μg/m^2) during this growth period t (s) from solutions with lower SI values (0.01–0.50) was less than 5% of the total calcite mass for each set of experiments (Table A1). Therefore, the surface coverage (η, Table A1) of calcite crystals on the sensor measured at the end of each set of experiment was used for growth rate (R, μmol/m^2/s) calculations, according to Eq. (2):

$$R = \Delta m / (5 M \eta t) \times 10^{-6} \quad (2)$$

where *M* is the molecular weight of calcite (100 g/mol)). As shown in Table 1, the QCM-D measured calcite growth rates increased with the increase of SI. For solutions with SI = −0.01 to 0.05 (Table 1), the differences in Ca^{2+} concentrations were within 5%, and such small differences could not be distinguished by ICP-MS. The observed calcite dissolution with SI = −0.01 (Fig. A1) and faster calcite growth at higher SI (Fig. 2a–e) indicated the consistency of our solution preparation and QCM-D measurements.

4. Discussion

4.1. Comparison of growth rates measured by QCM-D and other macroscopic measurements

A number of experiments have been performed to investigate the macroscopic growth rates of calcite using different measurement techniques, such as microbalance, auto-titration, and ICP-MS (Nancollas and Reddy, 1971, Reddy et al., 1981, Reddy and Gaillard, 1981, Zuddas and Mucci, 1994, Shiraki and Brantley, 1995, Zuddas and Mucci, 1998, Lin and Singer, 2005, Nehrke et al., 2007, Tang et al., 2008a, Tang et al., 2008b, Lopez et al., 2009, Gebrehiwet et al., 2012, Noiriel et al., 2012, Tang et al., 2012). Calcite reactive site densities and solution conditions (e.g., aqueous $\{Ca^{2+}\}/\{CO_3^{2-}\}$, temperature, background electrolytes, ionic strength, and solution pH) are widely known to affect calcite growth rates (Nehrke et al., 2007, Larsen et al., 2010a, Larsen et al., 2010b, Stack and Grantham, 2010, Gebrehiwet et al., 2012, Wolthers et al., 2012, Bracco et al., 2013, Stack, 2014). In some previous studies, the surface areas of calcite seed crystals or aqueous $\{Ca^{2+}\}/\{CO_3^{2-}\}$ were not clearly reported (Nancollas and Reddy, 1971, Reddy et al., 1981, Reddy and Gaillard, 1981, Lopez et al., 2009), or the reaction temperature was quite different from this study (Shiraki and Brantley, 1995). Thus, their reported growth rates cannot be compared with those measured in this study.

In the studies of Gebrehiwet et al., 2012, Nehrke et al., 2007, Lin and Singer, 2005, Zuddas and Mucci, 1998, and Noiriel et al. (2012), the $\{Ca^{2+}\}/\{CO_3^{2-}\}$ were reported (Table 2), and their experiments were conducted at similar temperatures (Table 2) to the present study. Their experimental pH conditions were also similar to this study (pH 8.16–9.01; Table 2), except for those of Nehrke et al. (2007) for which the pH was 10.2. The aqueous $\{Ca^{2+}\}/\{CO_3^{2-}\}$ was close to 1 in the study of Lin and Singer (2005) and varied in the other four studies (Zuddas and Mucci, 1998, Nehrke et al., 2007, Gebrehiwet et al., 2012, Noiriel et al., 2012). Using the relationship between aqueous $\{Ca^{2+}\}/\{CO_3^{2-}\}$ and calcite growth rate established by Nielsen et al. (2012) in the ion-by-ion model, the reported calcite growth rates from solutions with the same saturation index but with varied $\{Ca^{2+}\}/\{CO_3^{2-}\}$ were used to calculate the growth rates at $\{Ca^{2+}\}/\{CO_3^{2-}\} = 1$. The detailed calculations can be found in Appendix A. These recalculated rates at $\{Ca^{2+}\}/\{CO_3^{2-}\} = 1$ (Zuddas and Mucci, 1998, Nehrke et al., 2007, Gebrehiwet et al., 2012, Noiriel et al., 2012), as well as the rate measured by Lin and Singer (2005), are plotted in Fig. 4.

Table 2. Experimental conditions and recalculated calcite growth rates of previous macroscopic measurements.

References	pH	$\{Ca^{2+}\}/\{CO_3^{2-}\}$	SI	Ionic strength (M)	T (°C)	Electrolytes	Reported growth rates with varied $\{Ca^{2+}\}/\{CO_3^{2-}\}$ (R, μmol/m²/s)	Recalculated growth rate at $\{Ca^{2+}\}/\{CO_3^{2-}\} = 1$ (R, μmol/m²/s)
Gebrehiwet et al. (2012)	8.5	0.032	0.95	0.1	25	$CaCl_2$ $NaHCO_3$ KCl	0.69	1.16
Nehrke et al. (2007)	10.2	0.018	1.15		20	$CaCl_2$ K_2CO_3 NaCl	1.12	2.22
	10.2	0.022	0.70	0.1			1.05	1.80
Noiriel et al. (2012)	8.16	94.9	0.15	0.006–0.017	22	$CaCl_2$ $NaHCO_3$	0.0013	0.0023
	8.41	74.7	0.57				0.0055	0.0107
	8.25	70.9	0.42				0.0032	0.0060
	8.20	115	0.82				0.0123	0.0280
Lin and Singer (2005)	9.01	1.0	0.72	0.1	25	$CaCl_2$ Na_2CO_3 KCl	2.38	2.38
Zuddas and Mucci (1998)		3.3×10^3	0.15	0.1	25	$CaCl_2$ Na_2CO_3 NaCl $NaHCO_3$	0.0004	0.0018
		2.8×10^3	0.23				0.0005	0.0022
		2.6×10^3	0.25				0.0006	0.0026
		2.2×10^3	0.33				0.0006	0.0027
		1.5×10^3	0.48				0.0006	0.0025
		1.3×10^3	0.54				0.0007	0.0027
		1.2×10^3	0.60				0.0007	0.0026
		1.1×10^3	0.61				0.0007	0.0027
		0.9×10^3	0.70				0.0008	0.0029

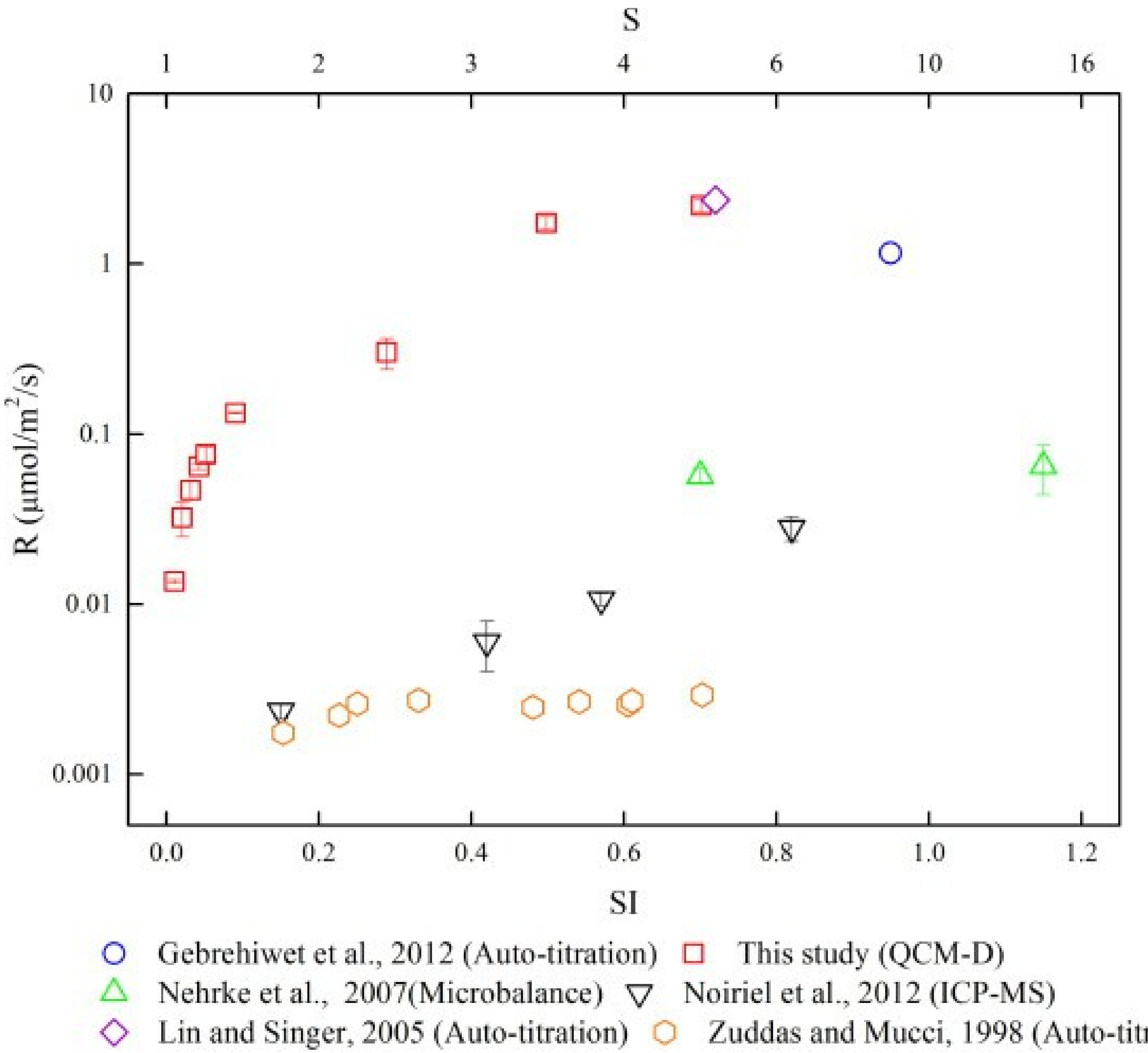

1. Download high-res image (275KB)
2. Download full-size image

Fig. 4. Calcite growth rates measured by QCM-D and other macroscopic techniques.

As shown in Fig. 4, the macroscopic growth rates measured by QCM-D (this study), Lin and Singer (2005), and Gebrehiwet et al. (2012) were similar, and were approximately 1.5 orders of magnitude higher than those measured by Nehrke et al. (2007), and were approximately two orders of magnitude higher than those measured by Noiriel et al. (2012) and Zuddas and Mucci (1998). The discrepancies could partly result from the differences in the electrolyte compositions, pH, temperature, and ionic strength of solutions (Table 2) (Ruiz-Agudo et al., 2011a, Ruiz-Agudo et al., 2011b). Moreover, these discrepancies might also result from the surface area normalization (Hodson, 2006). In Nehrke et al. (2007) and this study, the geometric surface area used for growth rate normalization was measured by optical microscopy; whereas Zuddas and Mucci, 1998, Lin and Singer, 2005, Gebrehiwet et al., 2012 and Noiriel et al. (2012) used specific surface areas measured by BET. Irrespective, the surface areas measured by either BET or microscope does not represent the real reactive site densities on mineral surfaces (Fischer et al., 2012). A systematic investigation of how to quantify surface reactive site densities is an important future direction but is not the focus of this paper.

4.2. Comparison of calcite growth rates measured by QCM-D and AFM

Many calcite growth experiments have been conducted using *in situ* AFM (Teng et al., 2000, Perdikouri et al., 2009, Larsen et al., 2010a, Larsen et al., 2010b, Stack and Grantham, 2010, Ruiz-Agudo et al., 2011a, Ruiz-Agudo et al., 2011b, Bracco et al., 2012, Bracco et al., 2013). Most of these studies used measured step velocities to determine spiral growth rates on the $10\bar{1}4$ surface (Teng et al., 2000, Ruiz-Agudo et al., 2011a, Bracco et al., 2013). To make these rates comparable with QCM-D data, the step velocity (v_s, m/s) and step density (ρ_{step}, µm^{-1}) measured by AFM on single spirals (Teng et al., 2000, Bracco et al., 2013) are needed to calculate the macroscopic calcite growth rate (*R*, µmol/m^2/s, Fig. 5) using Eq. (3):

$$R = \rho_{step} v_s h / V_m \times 10^9 \quad (3)$$

where V_m is the molar volume of calcite (36.93 cm^3/mol), *h* is the step height of an individual molecular layer (0.31 nm). Neither Larsen et al. (2010a) nor Perdikouri et al. (2009) reported step densities. Thus, those step velocities could not be converted to macroscopic growth rates. In the studies of Bracco et al., 2013, Teng et al., 2000, and Ruiz-Agudo et al. (2011a), step velocities with aqueous $\{Ca^{2+}\}/\{CO_3^{2-}\} \approx 1$ were measured using AFM. Step densities (ρ_{step}, µm^{-1}) were also measured and reported in Bracco et al. (2013) and Teng et al. (2000), whereas Ruiz-Agudo et al. (2011a) used an average value of 0.026 ± 0.015 to represent the slope (slope = $\rho_{step} \times h$) of the calcite surface, which can be used to calculate the step densities (ρ_{step}). Therefore, using the step velocity and step density values reported in these three studies, macroscopic calcite growth rates (*R*, µmol/m^2/s) were calculated using eqn. (4) and were compared with our QCM-D measurements (Fig. 5). In Bracco et al. (2013) and Ruiz-Agudo et al. (2011a), a K_{sp} value of $10^{-8.48}$ was used, the same as in this study. The SI values reported in Teng et al. (2000) were originally calculated with $K_{sp} = 10^{-8.54}$, but were recalculated here using $K_{sp} = 10^{-8.48}$.

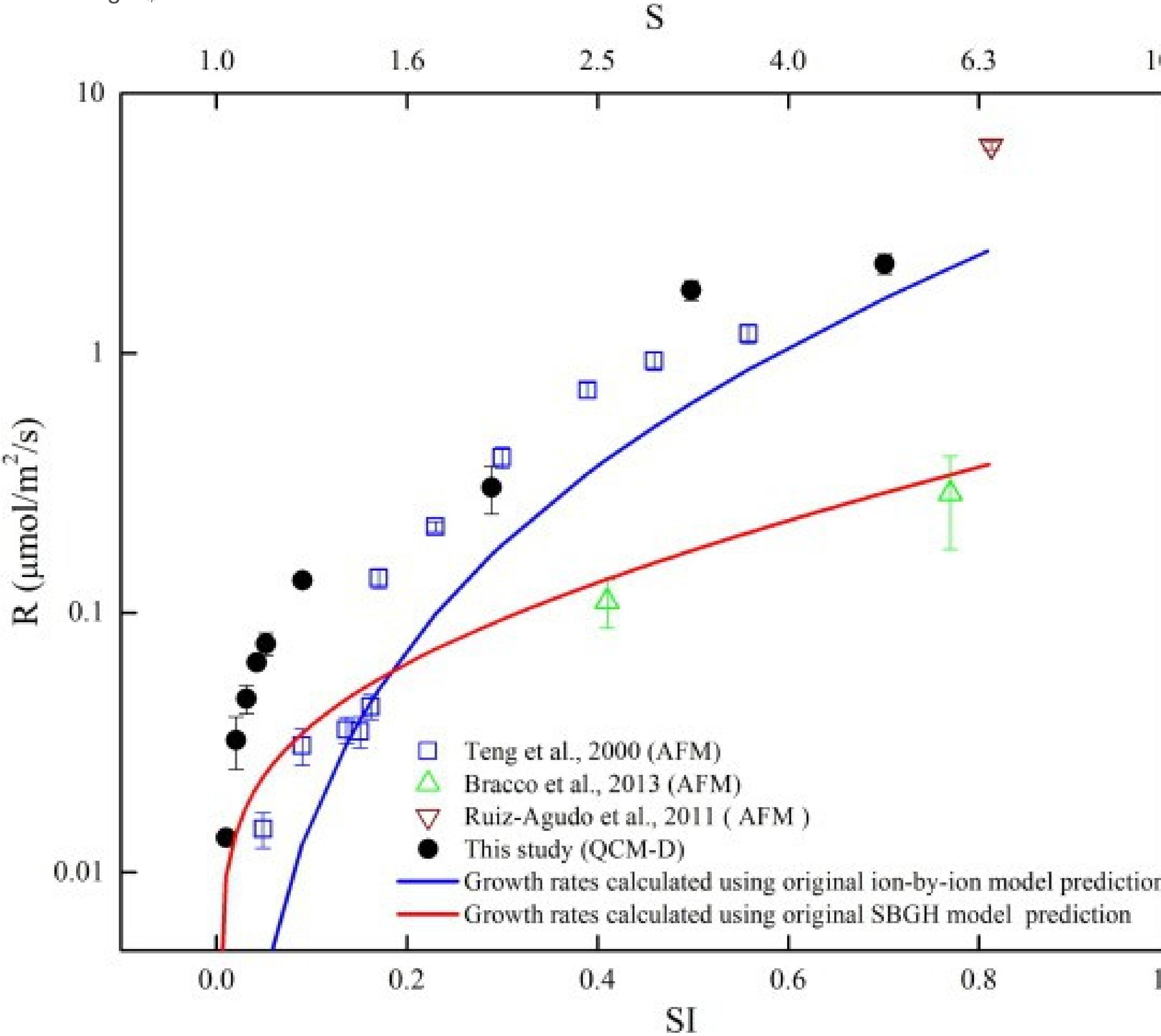

1. Download high-res image (316KB)
2. Download full-size image

Fig. 5. Calcite growth rates measured by QCM-D and AFM and predicted by the ion-by-ion and the SBGH models.

The macroscopic growth rates inferred from these *in situ* AFM studies (Fig. 5) were, in general, consistent with the rates measured by QCM-D (Fig. 5), validating that both QCM-D and *in situ* AFM can be used to accurately capture the macroscopic growth rate of calcite at low SI. This finding suggests that AFM can likely capture the representative growth mechanisms at low SI. As shown in Fig. 5, the growth rates measured by QCM-D in this study were in good agreement with those measured by Ruiz-Agudo et al. (2011a) and Teng et al. (2000) at SI > 0.10, and were approximately 2–5 times higher than those measured by Teng et al. (2000) at close to equilibrium conditions (SI < 0.1). Finally, our QCM-D derived rates and those of Teng et al. (2000) and Ruiz-Agudo et al. (2011a) were about one order of magnitude higher than those measured by Bracco et al. (2013).

As the growth rates (Fig. 5) were calculated using Eq. (3), the discrepancies in those growth rates could derive either from errors in step velocity or step density. Accordingly, the step velocities measured by AFM under similar SI conditions (Table 3) were compared. The obtuse step velocities reported by Bracco et al. (2013) and Teng et al. (2000) at SI ≈ 0.4 were quite similar, 7.89 and 8.10 nm/s (Table 3), respectively. The sum of obtuse and acute step velocities (V_{sum}, Table 3) measured by Bracco et al. (2013) and Ruiz-Agudo et al. (2011a) at SI ≈ 0.8 were also similar, 14.47 ± 3.3 and 10.14 ± 1.34 nm/s, respectively. The small discrepancies (within 40%) in measured step velocities of these calcite crystals growing from solutions under similar SI conditions might be attributed to the differences in solution pH and the composition and concentration of solution electrolytes (Detailed discussion in Appendix A).

Table 3. Experimental conditions, and the measured/calculated step velocities (v_s) and step densities (ρ_{step}) of calcite in previous AFM studies and the current QCM-D study.

References	pH	$\{Ca^{2+}\}/\{CO_3^{2-}\}$	SI	Ionic strength (M)	T (°C)	Electrolytes	Measured v_s (10^{-9} m/s)	Calculated v_s by SBGH model (10^{-9} m/s)	Calculated v_s by ion-by-ion model (10^{-9} m/s)	Measured ρ_{step}(μm^{-1})
Bracco et al. (2013)	9.07	1.27	0.77	0.005	N/A	$CaCl_2$ $NaHCO_3$	10.10 (v_{sum}:14.47)[a]	9.82	23.78	2.86
	8.68	1.02	0.41	0.004			7.89	5.08	8.20	1.41
Teng et al. (2000)	8.50	1.04	0.05	0.10	25	$CaCl_2$ $NaHCO_3$ NaCl	0.52	1.28	0.65	2.33
			0.09				1.18	1.78	1.25	2.27
			0.14				1.63	2.32	2.00	2.44
			0.15				1.89	2.42	2.24	1.96

References	pH	$\{Ca^{2+}\}/\{CO_3^{2-}\}$	SI	Ionic strength (M)	T (°C)	Electrolytes	Measured v_s (10^{-9} m/s)	Calculated v_s by SBGH model (10^{-9} m/s)	Calculated v_s by ion-by-ion model (10^{-9} m/s)	Measured ρ_{step} (μm^{-1})
			0.16				2.44	2.52	2.44	1.89
			0.17				2.52	2.62	2.60	4.00
			0.23				3.59	3.23	3.75	5.56
			0.30				5.18	3.93	5.31	7.14
			0.39				8.10	4.87	7.67	9.09
			0.46				9.46	5.64	9.84	11.11
			0.56				13.10	6.84	13.50	11.11
Ruiz-Agudo et al. (2011a,b)	8.50	1.00	0.81	0.10	25	$CaCl_2$ $NaHCO_3$ NaCl	10.14 (v_{sum})[a]	10.47	26.56	100.00
QCM-D	8.22	1.05	0.02	0.009	25	$CaCl_2$ $NaHCO_3$	1.99[b]	0.78	0.25	5.11
	8.22	1.05	0.10	0.010			2.62[b]	1.89	1.40	6.74
	8.21	1.02	0.30	0.013			3.10[b]	3.93	5.31	11.66
	8.20	1.07	0.50	0.017			11.20[b]	6.11	11.30	12.36

Note: v_s is the obtuse step velocity.

a

v_{sum} is the sum of obtuse and acute step velocity.

b

The step velocities were not directly measured but calculated using Eq. (4), as the step densities and growth rates were measured via VSI and QCM-D, respectively.

Considering the minor differences in measured step velocities (Table 3, within 40%), the much larger discrepancies in macroscopic growth rates among these previous AFM studies must mainly originate from differences in step densities of the calcite seed crystals. As shown in Table 3, the step density measured by Teng et al. (2000) at SI ≈ 0.40 was 9.09 μm^{-1}, 6.4 times larger than that measured by Bracco et al. (2013) at

1.41 μm^{-1}, whereas that reported by Ruiz-Agudo et al. (2011a) at SI ≈ 0.80 was 100 μm^{-1}, 36 times larger than that measured by Bracco et al. (2013) at 2.86 μm^{-1}.

The larger discrepancies in step densities were also the main cause of the growth rates differences between QCM-D and AFM measurements. Using the step densities measured by VSI (Fig. A6), the step velocities were calculated from QCM-D growth rates based on Eq. (4). These calculated step velocities (Table 3, 1.99 nm/s at SI = 0.10, 3.10 nm/s at SI = 0.30 and 11.20 nm/s at SI = 0.50) are within a factor of ∼1.1–1.6 of the values (Table 3, 1.18 nm/s at SI = 0.09, 5.18 nm/s at SI = 0.30, and 13.10 nm/s at SI = 0.56) reported in Teng et al. (2000), whereas larger difference existed in step densities. The measured step densities determined by VSI (Table 3, 5.11 μm^{-1} at SI = 0.10, 11.66 μm^{-1} at SI = 0.30 and 12.36 μm^{-1}at SI = 0.50) were ∼1.1–2.3 times the values (Table 3, 2.27 μm^{-1} at SI = 0.09, 7.14 μm^{-1} at SI = 0.30 and 11.11 μm^{-1} at SI = 0.56) reported in Teng et al. (2000) at similar SI conditions.

The significant differences in step densities of calcite crystals may be due to the application of different processes in the generation and pretreatment of calcite seed crystals among the various studies. In these previous AFM studies, Iceland spar calcite crystals were used, whereas, in the current QCM-D study, calcite seed crystals were generated on SAM coatings. Furthermore, different crystal pretreatments were used. Teng et al. (2000)pretreated their calcite crystals with a slightly supersaturated and near equilibrium solution for 1 h before the *in situ* AFM measurements. Bracco et al. (2013) pretreated their calcite crystals with an SI = 1.0 solution for 1 h, whereas Ruiz-Agudo et al. (2011a) did not pretreat their freshly-cleaved calcite crystals. In the current study, the seed crystal surfaces were pretreated with an SI = 0.7 solution. In the classical spiral growth model, the step spacing, the reciprocal of the step density, is determined by the critical step length at the top of the hillock, a function of the solution supersaturation with respect to calcite (Teng et al., 1998, Teng et al., 2000). To completely reset the step spacing of a given growth hillock, growth must proceed at a fixed SI for a sufficiently long time for the first step, nucleated under that condition, to propagate across the entire width of the growth hillock. The total time required to reset the step spacing will depend on the step velocity and the spacing (and thus size) of the growth hillocks. For example, Bracco et al. (2013) observed that after switching growth solutions of varied SIs, the step velocity of calcite could quickly (within 20 min) reach steady-state under different SI, while it took a much longer time (>40 min) for the step density to reach steady-state under some solution conditions, especially those with low calcium-to-carbonate ratios. In other words, the surface step density may not only be affected by the instantaneous solution saturation state but may also inherit step spacing from the previous solution, i.e., a memory artifact (Bracco et al., 2013, Stack, 2014). The use of different generation and pretreatment processes for calcite seed crystals used in these studies may have affected the step densities on the calcite crystals and therefore resulted in the discrepancies in the calculated macroscopic calcite growth rates. The comparison made here points out the importance of quantifying step densities for interpreting overall growth rates and sheds some light on the effects of pretreatment on step density.

4.3. Comparison of calcite growth rates measured by QCM-D and AFM with model predictions

Both macroscopic and microscopic models have been developed to describe calcite growth and dissolution processes (Burton et al., 1951, Zhang and Nancollas, 1990, Zuddas and Mucci, 1994, Zhang and Nancollas, 1998, Zuddas and Mucci, 1998, De Yoreo, 2003, De Yoreo et al., 2009, Andersson et al., 2016). Burton et al. (1951) developed the terrace-ledge-kink (TLK) theory, which was applied by Teng et al., 1998, Teng et al., 1999, Teng et al., 2000 and Larsen et al. (2010a) to model calcite growth from aqueous solutions. However, De Yoreo et al. (2009) pointed out that the application of TLK theory is not valid for calcite, as the kink formation rate limits calcite growth. Instead, a model of kink creation, propagation and collision (CPC), developed by Zhang and Nancollas, 1990, Zhang and Nancollas, 1998, is believed to capture the kink density-dependent growth rate of calcite accurately. More recently, Nielsen et al. (2012) developed an ion-by-ion model based on the CPC approach to predict calcite growth rates as a function of solution composition. Another process-based crystal growth model was also developed in previous studies, i.e., the Stack-Bracco-Grantham-Higgins (SBGH) model (Stack and Grantham, 2010, Bracco et al., 2012, Bracco et al., 2013, Bracco et al., 2016a, Bracco et al., 2016b). A third microkinetic model was developed by Andersson et al. (2016) to predict step velocity of calcite growth under varied aqueous conditions, but this model does not predict the step density and, thus, cannot estimate the macroscopic calcite growth rates as do the ion-by-ion and SBGH models. Therefore, only the ion-by-ion and SBGH model predictions were compared with the rates measured by QCM-D, and detailed descriptions of the two models are in Appendix A.

The growth rates predicted by the ion-by-ion (solid blue line in Fig. 6) and SBGH models (solid red line in Fig. 6) as a function of SI with $\{Ca^{2+}\}/\{CO_3^{2-}\} = 1$ were compared with the rates measured by QCM-D (black markers in Fig. 6). Both the ion-by-ion and SBGH models underpredicted the growth rates measured by QCM-D, especially at low SI.

Based on the discussion in Section 4.2, the discrepancies in calcite growth rates between measurements and model predictions may also arise mainly from the differences in step densities instead of step velocities. Therefore, steady-state step densities and step velocities predicted by both models (details of the calculation are provided in Appendix A) were compared with the QCM-D and VSI measurements (Table 3). Over the SI range of 0.02–0.50, differences in measured and predicted step velocities varied from 0.8 to 600% (Table 3); whereas the differences in measured and predicted step densities were much higher, varying from 87 to 1865% (Table 3). Similarly, the model predicted step velocities and step densities were compared with the AFM measurements (Table 3). Over the SI range of 0.05–0.56, differences in measured and model-predicted step velocities varied from 2 to 90% (Table 3), whereas the differences in measured and predicted step densities were much higher, varying from 25 to 270% (Table 3). This is because the step densities predicted by both models did not account for "memory effects" as discussed in Section 4.2. After crystal pretreatment, step velocities can quickly respond to changes in solution composition and could be predicted by both the ion-by-ion and SBGH models using the current solution compositions; whereas step densities require much longer time to reach a steady-state and could be significantly affected by the pretreatment procedures. The comparisons of model-predicted step densities and step velocities with AFM and QCM-D/VSI measurements confirmed the ability of both models to predict step velocities using the current solution conditions, meanwhile suggesting that better predictions could be achieved if transient-state step densities could be taken into account.

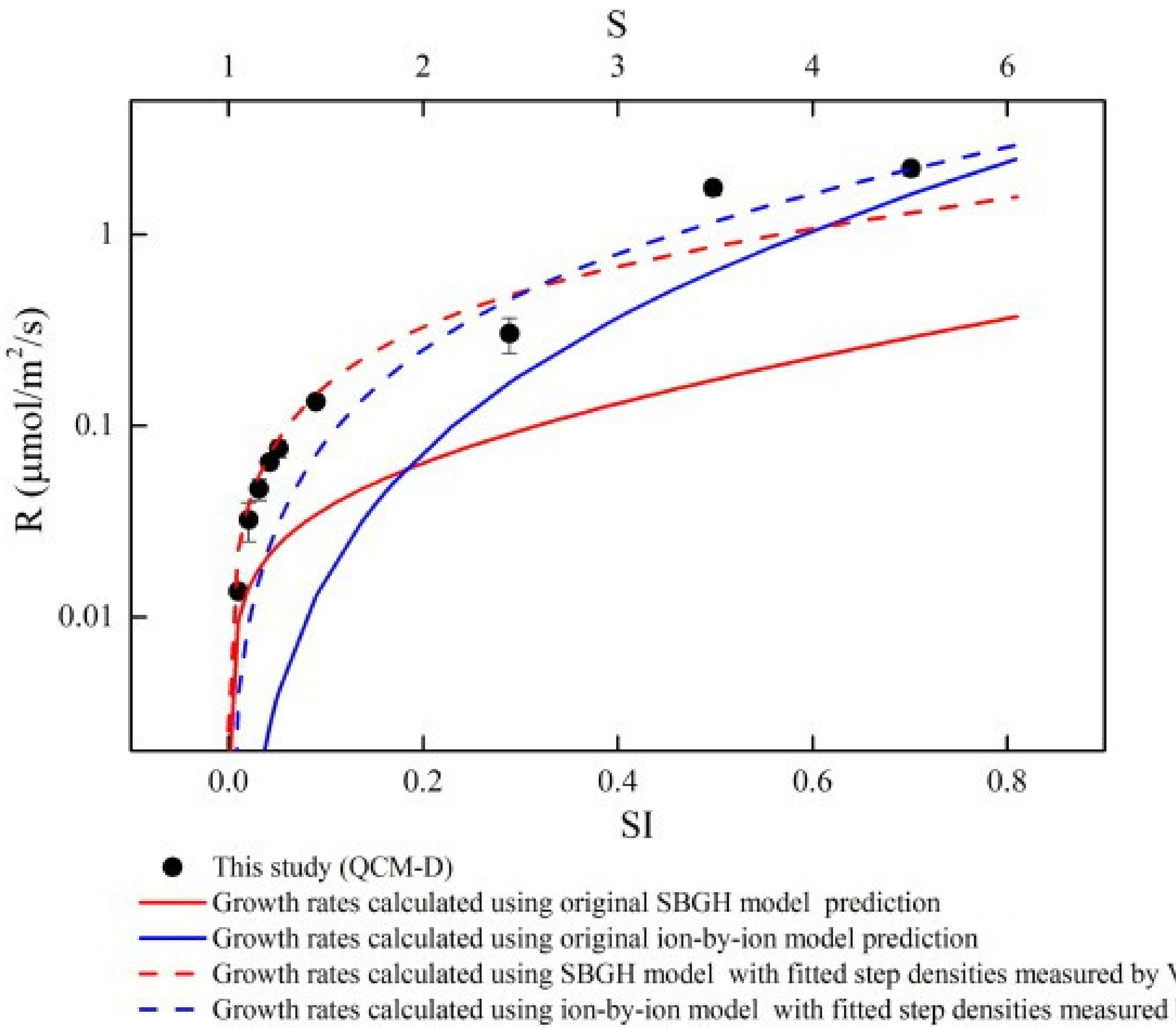

1. Download high-res image (383KB)
2. Download full-size image

Fig. 6. Calcite growth rates measured by QCM-D as well as predicted by the ion-by-ion and SBGH models.

As larger discrepancies in growth rates originated from differences in step densities, a second set of model calculations was conducted. The step densities measured by VSI were fitted as a function of SI (Fig. A6), and these were combined with the model predicted step velocities to calculate the growth rates using Eq. (4). Results of the calculation are plotted as dashed lines in Fig. 6. Compared with the original SBGH and ion-by-ion model predictions (solid red and blue lines, respectively) using predicted step densities, the modified predictions (dashed red and blue lines) using fitted step densities from VSI measurements agreed much better with the measured growth rates (black markers) by QCM-D (Fig. 6). The good agreement between the predictions using spiral-growth models (dashed lines in Fig. 6) and the QCM-D measurements also indicated that single-spiral growth was the dominant mechanism in our study for calcite growth under near-equilibrium conditions (i.e., low SI).

5. Conclusions

Quantitative determination of mineral precipitation rates is essential for successful prediction of the fate of nutrients and contaminants, as well as for the safety and efficiency of many surface and subsurface operations. For example, accurate prediction of calcium carbonateprecipitation rates is critical to determine the efficiency of sequestration of toxic metals such as strontium and selenium (Putnis et al., 2013), but the dearth of accurate growth rates at close to equilibrium conditions limits how well we can predict calcite precipitation at the reservoir scale using reactive transport modeling. In this study, QCM-D was successfully applied for the first time to quantify macroscopic calcite growth rates at atmospheric pressure under close to equilibrium conditions, and the method developed was validated with traditional techniques. This novel method can be adopted for many different applications and could greatly benefit both the geochemistry and nanochemistry communities.

The calcite growth rates measured by QCM-D were compared with results of previous studies using other macroscopic and microscopic techniques, as well as with ion-by-ion and SBGH model predictions. Whereas discrepancies between experimental and model results will not be resolved in a single study, the present study provides valuable insights on the importance of reactive site density in the quantification of calcite growth rates and illustrates the importance of coupling macroscopic and microscopic rate data to interpret these rates accurately. Nevertheless, the agreement between growth rates measured by QCM-D, AFM and model predictions using steady-state step velocities and the measured step densities highlight the ability of these models to predict calcite growth rates. The discrepancy among the measured and the predicted step densities likely result from a memory artifact, i.e., step density was not only controlled by the reactive solution composition but also affected by the pretreatment solution conditions. The memory artifact implies that a revised model, which considers not only the steady-state step density but also the transient-state step density changes after solution condition changes, could predict better calcite growth rates. A systematic investigation of the effects of pretreatment solution conditions on step densities of calcite seed crystals, which could help design such models, is an important future direction of research.

Acknowledgments

This work was supported by the Center for Nanoscale Control of Geologic CO_2, an Energy Frontier Research Center funded by the U.S. Department of Energy, Office of Science, Basic Energy Sciences under Contract No. DE-AC02-05CH11231 to Lawrence Berkeley National Laboratory. We thank Dr. Namhey Lee and Dr. Kevin Knauss for helping with VSI measurements and Dr. Mariëtte Wolthers for sharing the recalculated growth data of Nehrke et al. (2007).

Appendix A. Supplementary material

Download Word document (3MB)Help with docx files

Supplementary data 1.

References

Aizenberg et al., 1999a

J. Aizenberg, A.J. Black, G.M. Whitesides**Control of crystal nucleation by patterned self-assembled monolayers**

Nature, 398 (1999), pp. 495-498

CrossRefView Record in Scopus

Aizenberg et al., 1999b

J. Aizenberg, A.J. Black, G.H. Whitesides**Oriented growth of calcite controlled by self-assembled monolayers of functionalized alkanethiols supported on gold and silver**

J. Am. Chem. Soc., 121 (1999), pp. 4500-4509

CrossRefView Record in Scopus

Andersson et al., 2016

M.P. Andersson, S. Dobberschütz, K.K. Sand, D.J. Tobler, J.J. De Yoreo, S.L.S. Stipp**A Microkinetic model of calcite step growth**

Angew. Chem., 128 (2016), pp. 11252-11256

CrossRefView Record in Scopus

Bracco et al., 2016a

J.N. Bracco, Y. Gooijer, S.R. Higgins**Growth kinetics of step edges on celestite (001) surfaces as a function of temperature, saturation state, ionic strength, and aqueous strontium: sulfate ratio: an in-situ atomic force microscopy study**

Geochim. Cosmochim. Acta, 175 (2016), pp. 222-238

ArticleDownload PDFView Record in Scopus

Bracco et al., 2016b

J.N. Bracco, Y. Gooijer, S.R. Higgins**Hydrothermal atomic force microscopy observations of barite step growth rates as a function of the aqueous barium-to-sulfate ratio**

Geochim. Cosmochim. Acta, 183 (2016), pp. 1-13

ArticleDownload PDFView Record in Scopus

Bracco et al., 2012

J.N. Bracco, M.C. Grantham, A.G. Stack**Calcite growth rates as a function of aqueous calcium-to-carbonate ratio, saturation index, and inhibitor concentration: insight into the mechanism of reaction and poisoning by strontium**

Cryst. Growth Des., 12 (2012), pp. 3540-3548

CrossRefView Record in Scopus

Bracco et al., 2013

J.N. Bracco, A.G. Stack, C.I. Steefel**Upscaling calcite growth rates from the mesoscale to the macroscale**

Environ. Sci. Technol., 47 (2013), pp. 7555-7562

CrossRefView Record in Scopus

Burton et al., 1951

W.K. Burton, N. Cabrera, F.C. Frank**The growth of crystals and the equilibrium structure of their surfaces**

Philos. Trans. R. Soc. London, Ser. A, 243 (1951), pp. 299-358

CrossRefView Record in Scopus

Chen et al., 2016

Q. Chen, S. Xu, Q. Liu, J. Masliyah, Z. Xu**QCM-D study of nanoparticle interactions**

Adv. Colloid Interface Sci., 233 (2016), pp. 94-114

ArticleDownload PDFView Record in Scopus

Christoffersen and Christoffersen, 1990

J. Christoffersen, M.R. Christoffersen**Kinetics of spiral growth of calcite crystals and determination of the absolute rate-constant**

J. Cryst. Growth, 100 (1990), pp. 203-211

ArticleDownload PDFView Record in Scopus

Dai and Hu, 2014

C. Dai, Y. Hu**Fe(III) Hydroxide nucleation and growth on quartz in the presence of Cu(II), Pb(II), and Cr(III): metal hydrolysis and adsorption**

Environ. Sci. Technol., 49 (2014), pp. 292-300

Dai et al., 2016a

C. Dai, A.G. Stack, A. Koishi, A. Fernandez-Martinez, S.S. Lee, Y. Hu**Heterogeneous nucleation and growth of barium sulfate at organic–water interfaces: interplay between surface hydrophobicity and Ba^{2+} adsorption**
Langmuir, 32 (2016), pp. 5277-5284
CrossRefView Record in Scopus

Dai et al., 2016b

C. Dai, X. Zuo, B. Cao, Y. Hu**Homogeneous and heterogeneous $(Fe_x, Cr_{1-x})(OH)_3$ precipitation: implications for Cr sequestration**
Environ. Sci. Technol., 50 (2016), pp. 1741-1749
CrossRefView Record in Scopus

De Yoreo, 2003

J.J. De Yoreo**Principles of crystal nucleation and growth**
Rev. Mineral. Geochem., 54 (2003), pp. 57-93
CrossRefView Record in Scopus

De Yoreo et al., 2009

J.J. De Yoreo, L.A. Zepeda-Ruiz, R.W. Friddle, S.R. Qiu, L.E. Wasylenki, A.A. Chernov, G.H. Gilmer, P.M. Dove**Rethinking classical crystal growth models through molecular scale insights: consequences of kink-limited kinetics**
Cryst. Growth Des., 9 (2009), pp. 5135-5144
CrossRefView Record in Scopus

Dixon, 2008

M.C. Dixon**Quartz crystal microbalance with dissipation monitoring: enabling real-time characterization of biological materials and their interactions**

J. Biomo. Tech., 19 (2008), pp. 151-158

View Record in Scopus

Eisenhauer et al

A. Eisenhauer, B. Kisakurek, F. Bohm**Marine calcification: an alkali earth metal isotope perspective**

Elements, 5 (2009), pp. 365-368

CrossRefView Record in Scopus

Fantle and DePa

M.S. Fantle, D.J. DePaolo**Variations in the marine Ca cycle over the past 20 million years**

Earth Planet. Sci. Lett., 237 (2005), pp. 102-117

ArticleDownload PDFView Record in Scopus

Fischer et al., 20

C. Fischer, R.S. Arvidson, A. Luettge**How predictable are dissolution rates of crystalline material?**

Geochim. Cosmochim. Acta, 98 (2012), pp. 177-185

ArticleDownload PDFView Record in Scopus

Gebrehiwet et al

T.A. Gebrehiwet, G.D. Redden, Y. Fujita, M.S. Beig, R.W. Smith**The effect of the CO_3^{2-} to Ca^{2+} ion activity ratio on calcite precipitation kinetics and Sr^{2+}partitioning**

Geochem. Trans., 13 (2012)

Gratz et al., 1993

A.J. Gratz, P.E. Hillner, P.K. Hansma**Step dynamics and spiral growth on calcite**

Geochim. Cosmochim. Acta, 57 (1993), pp. 491-495

ArticleDownload PDFView Record in Scopus

Hodson, 2006

M.E. Hodson**Searching for the perfect surface area normalizing term—a comparison of BET surface area-, geometric surface area-and mass-normalized dissolution rates of anorthite and biotite**

J. Geochem. Explor., 88 (2006), pp. 288-291

ArticleDownload PDFView Record in Scopus

Höök et al., 2008

F. Höök, B. Kasemo, M. Grunze, S. Zauscher**Quantitative biological surface science: challenges and recent advances**

ACS Nano, 2 (2008), pp. 2428-2436

View Record in Scopus

Icenhower and S

J.P. Icenhower, C.I. Steefel**Dissolution rate of borosilicate glass SON68: a method of quantification based upon interferometry and implications for experimental and natural weathering rates of glass**
Geochim. Cosmochim. Acta, 157 (2015), pp. 147-163
ArticleDownload PDFView Record in Scopus

Knoll et al., 2008

W. Knoll, I. Köper, R. Naumann, E.-K. Sinner**Tethered bimolecular lipid membranes—a novel model membrane platform**
Electrochim. Acta, 53 (2008), pp. 6680-6689
ArticleDownload PDFView Record in Scopus

Lagneau et al., 2

V. Lagneau, A. Pipart, H. Catalette**Reactive transport modeling and long term behaviour of CO_2 sequestration in saline aquifers**
Oil Gas Sci. Technol., 60 (2005), pp. 231-247
CrossRefView Record in Scopus

Larsen et al., 20

K. Larsen, K. Bechgaard, S.L.S. Stipp**The effect of the Ca^{2+} to CO_3^{2-} activity ratio on spiral growth at the calcite 1014 surface**
Geochim. Cosmochim. Acta, 74 (2010), pp. 2099-2109
ArticleDownload PDFView Record in Scopus

Larsen et al., 20

K. Larsen, K. Bechgaard, S.L.S. Stipp**Modelling spiral growth at dislocations and determination of critical step lengths from pyramid geometries on calcite 1014 surfaces**
Geochim. Cosmochim. Acta, 74 (2010), pp. 558-567
ArticleDownload PDFView Record in Scopus

Lin and Singer, 2

Y.P. Lin, P.C. Singer**Effects of seed material and solution composition on calcite precipitation**
Geochim. Cosmochim. Acta, 69 (2005), pp. 4495-4504
ArticleDownload PDFView Record in Scopus

Lopez et al., 200

O. Lopez, P. Zuddas, D. Faivre**The influence of temperature and seawater composition on calcite crystal growth mechanisms and kinetics: implications for Mg incorporation in calcite lattice**
Geochim. Cosmochim. Acta, 73 (2009), pp. 337-347
ArticleDownload PDFView Record in Scopus

Maroni et al., 20

P. Maroni, F.J. Montes Ruiz-Cabello, C. Cardoso, A. Tiraferri**Adsorbed mass of polymers on self-assembled monolayers: effect of surface chemistry and polymer charge**

Langmuir, 31 (2015), pp. 6045-6054
CrossRefView Record in Scopus

Marshall and Mc

J.F. Marshall, M.T. McCulloch**An assessment of the Sr/Ca ratio in shallow water hermatypic corals as a proxy for sea surface temperature**
Geochim. Cosmochim. Acta, 66 (2002), pp. 3263-3280
ArticleDownload PDFView Record in Scopus

Morse and Arvids

J.W. Morse, R.S. Arvidson**The dissolution kinetics of major sedimentary carbonate minerals**
Earth Sci. Rev., 58 (2002), pp. 51-84
ArticleDownload PDFView Record in Scopus

Morse et al., 200

J.W. Morse, R.S. Arvidson, A. Luttge**Calcium carbonate formation and dissolution**
Chem. Rev., 107 (2007), pp. 342-381
CrossRefView Record in Scopus

Nancollas and R

G.H. Nancollas, M.M. Reddy**The crystallization of calcium carbonate. II. Calcite growth mechanism**
J. Colloid Interface Sci., 37 (1971), pp. 824-830
ArticleDownload PDFView Record in Scopus

Nehrke et al., 20

G. Nehrke, G.J. Reichart, P. Van Cappellen, C. Meile, J. Bijma**Dependence of calcite growth rate and Sr partitioning on solution stoichiometry: Non-Kossel crystal growth**
Geochim. Cosmochim. Acta, 71 (2007), pp. 2240-2249
ArticleDownload PDFView Record in Scopus

Nielsen et al., 20

L.C. Nielsen, D.J. DePaolo, J.J. De Yoreo**Self-consistent ion-by-ion growth model for kinetic isotopic fractionation during calcite precipitation**
Geochim. Cosmochim. Acta, 86 (2012), pp. 166-181
ArticleDownload PDFView Record in Scopus

Noiriel et al., 201

C. Noiriel, C.I. Steefel, L. Yang, J. Ajo-Franklin**Upscaling calcium carbonate precipitation rates from pore to continuum scale**
Chem. Geol., 318 (2012), pp. 60-74
ArticleDownload PDFView Record in Scopus

Perdikouri et al.,

C. Perdikouri, C.V. Putnis, A. Kasioptas, A. Putnis**An atomic force microscopy study of the growth of a calcite surface as a function of calcium/total carbonate concentration ratio in solution at constant supersaturation**

Cryst. Growth Des., 9 (2009), pp. 4344-4350
CrossRefView Record in Scopus

Plummer, 1975

L.N. Plummer**Mixing of sea water with calcium carbonate ground water**
Geol. Soc. Am. Mem., 142 (1975), pp. 219-236
View Record in Scopus

Plummer and Bu

L.N. Plummer, E. Busenberg**The solubilities of calcite, aragonite and vaterite in CO_2-H_2O solutions between 0 and 90 °C, and an evaluation of the aqueous model for the system $CaCO_3$-CO_2-H_2O**
Geochim. Cosmochim. Acta, 46 (1982), pp. 1011-1040
ArticleDownload PDFView Record in Scopus

Putnis et al., 201

C.V. Putnis, F. Renard, H.E. King, G. Montes-Hernandez, E. Ruiz-Agudo**Sequestration of selenium on calcite surfaces revealed by nanoscale imaging**
Environ. Sci. Technol., 47 (2013), pp. 13469-13476
CrossRefView Record in Scopus

Reddy and Gailla

M.M. Reddy, W.D. Gaillard**Kinetics of calcium carbonate (calcite)-seeded crystallization: influence of solid/solution ratio on the reaction rate constant**
J. Colloid Interface Sci., 80 (1981), pp. 171-178
ArticleDownload PDFView Record in Scopus

Reddy et al., 198

M.M. Reddy, L.N. Plummer, E. Busenberg**Crystal growth of calcite from calcium bicarbonate solutions at constant P_{CO_2} and 25 °C: a test of a calcite dissolution model**
Geochim. Cosmochim. Acta, 45 (1981), pp. 1281-1289
ArticleDownload PDFView Record in Scopus

Richter and Briss

R.P. Richter, A. Brisson**QCM-D on mica for parallel QCM-D AFM studies**
Langmuir, 20 (2004), pp. 4609-4613
CrossRefView Record in Scopus

Ruiz-Agudo et al

E. Ruiz-Agudo, C.V. Putnis, C. Rodriguez-Navarro, A. Putnis**Effect of pH on calcite growth at constant ratio and supersaturation**
Geochim. Cosmochim. Acta, 75 (2011), pp. 284-296
ArticleDownload PDFView Record in Scopus

Ruiz-Agudo et al., 2011b

E. Ruiz-Agudo, C.V Putnis, L. Wang, A. Putnis**Specific effects of background electrolytes on the kinetics of step propagation during calcite growth**

Geochim. Cosmochim. Acta, 75 (2011), pp. 3803-3814
ArticleDownload PDFView Record in Scopus
Shiraki and Brantley, 1995
R. Shiraki, S.L. Brantley**Kinetics of near-equilibrium calcite precipitation at 100°C: an evaluation of elementary reaction-based and affinity-based rate laws**
Geochim. Cosmochim. Acta, 59 (1995), pp. 1457-1471
ArticleDownload PDFView Record in Scopus
Stack, 2014
A.G. Stack**Next generation models of carbonate mineral growth and dissolution**
Greenhouse Gases Sci. Technol., 4 (2014), pp. 278-288
CrossRefView Record in Scopus
Stack and Grantham, 2010
A.G. Stack, M.C. Grantham**Growth rate of calcite steps as a function of aqueous calcium-to-carbonate ratio: independent attachment and detachment of calcium and carbonate Ions**
Cryst. Growth Des., 10 (2010), pp. 1409-1413
CrossRefView Record in Scopus
Steefel et al., 2005
C. Steefel, D. Depaolo, P. Lichtner**Reactive transport modeling: an essential tool and a new research approach for the Earth sciences**
Earth Planet. Sci. Lett., 240 (2005), pp. 539-558
ArticleDownload PDFView Record in Scopus
Tang et al., 2008a
J. Tang, M. Dietzel, F. Boehm, S.J. Koehler, A. Eisenhauer**Sr^{2+}/Ca^{2+} and $^{44}Ca/^{40}Ca$ fractionation during inorganic calcite formation: II. Ca isotopes**
Geochim. Cosmochim. Acta, 72 (2008), pp. 3733-3745
ArticleDownload PDFView Record in Scopus
Tang et al., 2008b
J. Tang, S.J. Köhler, M. Dietzel**Sr^{2+}/Ca^{2+} and $^{44}Ca/^{40}Ca$ fractionation during inorganic calcite formation: I. Sr incorporation**
Geochim. Cosmochim. Acta, 72 (2008), pp. 3718-3732
ArticleDownload PDFView Record in Scopus
Tang et al., 2012
J. Tang, A. Niedermayr, S.J. Köhler, F. Böhm, B. Kısakürek, A. Eisenhauer, M. Dietzel**Sr^{2+}/Ca^{2+} and $^{44}Ca/^{40}Ca$ fractionation during inorganic calcite formation: III. Impact of salinity/ionic strength**
Geochim. Cosmochim. Acta, 77 (2012), pp. 432-443
ArticleDownload PDFView Record in Scopus
Teng et al., 1998

H.H. Teng, P.M. Dove, C.A. Orme, J.J. De Yoreo**Thermodynamics of calcite growth: baseline for understanding biomineral formation**
Science, 282 (1998), pp. 724-727
CrossRefView Record in Scopus
Teng et al., 1999
H.H. Teng, P.M. Dove, J.J. DeYoreo**Reversed calcite morphologies induced by microscopic growth kinetics: insight into biomineralization**
Geochim. Cosmochim. Acta, 63 (1999), pp. 2507-2512
ArticleDownload PDFView Record in Scopus
Teng et al., 2000
H.H. Teng, P.M. Dove, J.J. De Yoreo**Kinetics of calcite growth: surface processes and relationships to macroscopic rate laws**
Geochim. Cosmochim. Acta, 64 (2000), pp. 2255-2266
ArticleDownload PDFView Record in Scopus
Teng et al., 2011
H.H. Teng, P.M. Dove, J.J.De Yoreo**The kinetics of calcite growth: Interpreting chemical affinity-based rate laws through the lens of direct observation**
MRS Proc., 620 (2011)
Tucker and Wright, 1990
M.E. Tucker, V.P. Wright**Carbonate Mineralogy and Chemistry**
Blackwell Publishing Ltd., Oxford, UK (1990), pp. 284-313
CrossRefView Record in Scopus
Voinova et al., 1999
M.V. Voinova, M. Rodahl, M. Jonson, B. Kasemo**Viscoelastic acoustic response of layered polymer films at fluid-solid interfaces: continuum mechanics approach**
Phys. Scr., 59 (1999), pp. 391-396
CrossRefView Record in Scopus
Wang et al., 2010
X. Wang, E. Ingall, B. Lai, A.G. Stack**Self-assembled monolayers as templates for heme crystallization**
Cryst. Growth Des., 10 (2010), pp. 798-805
CrossRefView Record in Scopus
Wolthers et al., 2012
M. Wolthers, G. Nehrke, J.P. Gustafsson, P. Van Cappellen**Calcite growth kinetics: modeling the effect of solution stoichiometry**
Geochim. Cosmochim. Acta, 77 (2012), pp. 121-134
ArticleDownload PDFView Record in Scopus
Zhang and Nancollas, 1990

J. Zhang, G.H. Nancollas**Kink densities along a crystal surface step at low temperatures and under nonequilibrium conditions**

J. Cryst. Growth, 106 (1990), pp. 181-190

ArticleDownload PDFView Record in Scopus

Zhang and Nancollas, 1998

J.W. Zhang, G.H. Nancollas**Kink density and rate of step movement during growth and dissolution of an AB crystal in a nonstoichiometric solution**

J. Colloid Interface Sci., 200 (1998), pp. 131-145

ArticleDownload PDFView Record in Scopus

Zhong and Mucci, 1993

S.J. Zhong, A. Mucci**Calcite precipitation in seawater using a constant addition technique - a new overall reaction kinetic expression**

Geochim. Cosmochim. Acta, 57 (1993), pp. 1409-1417

Zhu et al., 2016

Z. Zhu, V.G. Hadjiev, Y. Rong, R. Guo, B. Cao, Z. Tang, F. Qin, Y. Li, Y. Wang, F. Hao**Interaction of organic cation with water molecule in perovskite MAPbI3: from dynamic orientational disorder to hydrogen bonding**

Chem. Mater., 28 (2016), pp. 7385-7393

CrossRefView Record in Scopus

Zuddas and Mucci, 1994

P. Zuddas, A. Mucci**Kinetics of calcite precipitation from seawater: I. A classical chemical kinetics description for strong electrolyte solutions**

Geochim. Cosmochim. Acta, 58 (1994), pp. 4353-4362

ArticleDownload PDFView Record in Scopus

Zuddas and Mucci, 1998

P. Zuddas, A. Mucci**Kinetics of calcite precipitation from seawater: II. The influence of the ionic strength**

Geochim. Cosmochim. Acta, 62 (1998), pp. 757-766

ArticleDownload PDFView Record in Scopus